Int. J. Multiphase Flow Vol. 16, No. 3, pp. 529–543, 1990
Printed in Great Britain.

0301-9322/90 $3.00 + 0.00

A BOUNDARY INTEGRAL EQUATION SOLUTION OF THE STOKES FLOW DUE TO THE MOTION OF AN ARBITRARY BODY NEAR A PLANE WALL WITH A HOLE

E. GAVZE
Department of Atmospheric Sciences, The Hebrew University of Jerusalem, Jerusalem 91904, Israel

(*Received* 4 *December* 1987; *in revised form* 5 *January* 1990)

Abstract—A boundary integral equation technique is presented for solving the low Reynolds number hydrodynamic interaction of a rigid body with a plane wall and a hole. Such a problem occurs during the process of filtration by a multipore or similar devices. The proposed technique utilizes the Green function of the Stokes equation for the infinite plane wall to eliminate all unknowns on the plane wall. A system of two integral equations is derived, for the stresses on the surface of the body and for the velocity in the hole; this system is later reduced to a single equation. The proposed technique is applicable to a hole and a body of arbitrary shape and no symmetry is required.

Key Words: Stokes flow, filtration flow, boundary integral equation

1. INTRODUCTION

The motion of a particle in the vicinity of a pore is of interest in investigating filtration and sampling of aerosols by a multipore. A particle moving near a wall is subjected to additional force and torque, known altogether as the "wall effect". These forces are due to the stresses formed on the wall. The presence of a hole in the wall adds to the complexity of the problem, in that the symmetry is distorted and the particle experiences a different force as its distance from the hole and direction of motion change.

Dagan *et al.* (1982a) have shown that, in the absence of additional boundaries, the flow through a circular orifice is little affected by its thickness. In most papers treating this problem, zero wall thickness has been assumed. Davis *et al.* (1981) solved the axisymmetric problem of a point force approaching a circular hole along its symmetry axis by solving a dual integral equation on the wall, with an additional correction velocity term in the hole. Davis (1983) obtained results for the same problem, correct to the third order of the sphere's radius. His results agree well with later results for a sphere-to-hole radii ratio up to about 1. Dagan *et al.* (1982b) solved the same problem, but for a sphere of finite size, by constructing two different axisymmetric solutions, of Fourier–Bessel type, for both sides of the wall and matching them by requiring the continuity of the velocity and the normal components of the stress tensor across the hole. Their solution is given as truncated infinite series whose coefficients are determined by the satisfaction of the boundary conditions on a finite number of points on the sphere's surface (Ganatos *et al.* 1980). Miyazaki & Hasimoto (1984) obtained a closed-form solution for a point force of arbitrary position and direction of motion in the vicinity of a circular hole. Recently, Yan *et al.* (1987) applied a combined infinite series–integral equation method for the arbitrary motion of a finite sphere near a circular hole. In their solution, the velocity is given as a sum of the single-layer potential with the stress on the wall and an infinite series of spherical harmonics. The satisfaction of the boundary conditions and the truncation of the series and the infinite wall lead to a finite set of linear equations. All the above-mentioned solutions apply to cases in which a certain symmetry is required from the body. Dagan *et al.* (1983) calculated the trajectories of neutrally buoyant and inertialess spheres which approach a circular hole in low Reynolds numbers. They used an order of magnitude analysis to estimate the hydrodynamic interaction of the spheres with the boundaries. They compared their calculations to experimental results and found good agreement. In a later paper, Wang *et al.* (1986) studied the same problem but without neglecting the particles' inertia, with improved estimates of the

hydrodynamic interaction and with molecular attraction of the wall. These last two papers demonstrated the importance of the hydrodynamic interaction which, eventually, caused all the particles to enter the hole (in the absence of molecular forces). Dagan *et al.* (1988) dealt with the axisymmetric motion of a gas bubble at the exit of a circular orifice in the presence of a stagnant cap of insoluble surfactants. The unknown stresses and velocities on the surface of the drop were approximated by piecewise quadratic functions. The use of the multipole-series technique, as in Yan *et al.* (1987), required a great number of terms, due to the discontinuity of the velocity on the surface of the drop, and proved to be inefficient.

On studying the problem we decided to develop a method for which no symmetry is required and for which the domain of integration does not have to be truncated. In formulating the problem, in the general non-symmetric case, as a boundary integral equation, two approaches may be taken. One may, as in Yan *et al.* (1987), represent the solution directly as a single-layer potential on the infinite wall and on the body's surface (see Ladyzhenskaya 1963) (the double-layer potential on the body's surface vanishes identically for rigid-body motions) and solve the equations for the stress on both surfaces. This approach has the advantage that the body can cross the hole's plane, but the disadvantage that the infinite wall has to be truncated. This may become an acute problem when different positions of the body, relative to the wall, are considered so that different truncations have to be made each time. Another approach, the Green function approach, taken by us, is to represent the solution with the aid of the Green function for the infinite plane wall. In this representation, both single- and double-layer potentials vanish on the wall and one is left with the single-layer potential on the body's surface and the double-layer potential, with the unknown fluid velocity, on the hole's plane. Two different solutions are constructed for the half space $z > 0$ and $z < 0$ (figure 1), and equations are obtained by requiring the continuity of the velocity and the normal components of the stress tensor. The body can now be placed as far from the hole as necessary without having to modify the domain of integration. The main disadvantage of this proposed technique is that the body can not intersect the plane of the hole but, as we show, good accuracy is achieved even with a distance/radius ratio of 1.1, so that practically there are no limitations in calculating the trajectories of particles approaching the hole.

In this paper we present results for spheres and for elongated ellipsoids. The results for spheres are in good agreement with previous results except for the transverse components of the force near the hole, for which our results are up to one order of magnitude higher than the results of Yan *et al.* (1987); this demonstrates the importance of the hydrodynamic interaction with the boundaries. The results for the ellipsoids are, to the best of our knowledge, the first to be reported in the literature.

2. DERIVATION OF THE BOUNDARY INTEGRAL EQUATIONS

Assuming the Reynolds number with respect to the body and the hole is small, $\mathrm{Re} \ll 1$, the flow, generated by the body's motion is considered a Stokes flow. We adopt the quasi-stationary assumption, according to which the flow is considered steady at every moment and the velocity of the body is taken to be the boundary conditions for the flow at the body's surface Σ_1. Using the reciprocal theorem for Stokes flow it may be shown that, knowing the stresses on Σ_1, arising from the six independent translations and rotations of the rigid body, the force and the torque on the body can be calculated for any Stokes flow in the same geometry.

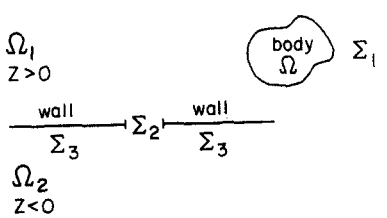

Figure 1. The geometry of the problem.

The governing equation is therefore the Stokes equation, written for viscosity $\mu = 1$:

$$\Delta V_i = \frac{\partial p}{\partial x_i}, \qquad \frac{\partial V_i}{\partial x_i} = 0;$$
$$V_i|_{\Sigma_1} = V_i^0, \qquad V_i|_{\Sigma_3} = 0; \tag{1}$$

where V_i is the velocity of the fluid and V_i^0 is the velocity of the body. The fundamental solution of Stokes equation is

$$U_{ij}(x, y) = \frac{1}{8\pi}\left[\frac{\delta_{ij}}{|x-y|} + \frac{(x_i - y_i)(x_j - y_j)}{|x-y|^3}\right],$$
$$q_i(x, y) = \frac{1}{4\pi}\frac{y_i - x_i}{|x-y|^3}. \tag{2}$$

X and Y are two field points and $|x-y|$ is the Euclidean distance between them. (U, q) satisfy [1] with respect to Y and $(U, -q)$ with respect to X. The stress tensor for the flow (V, p) is

$$\sigma_{ij}(V, p) = \frac{\partial V_i}{\partial x_j} + \frac{\partial V_j}{\partial x_i} - \delta_{ij} p. \tag{3}$$

$U_{ij}(x, y)$ is the kernel of the single-layer potential. The kernel of the double-layer potential is the stress tensor of the fundamental solution (U, q):

$$\sigma_{ij}(U_k, q_k)_y = \frac{3}{4\pi}\frac{(x_i - y_i)(x_j - y_j)(x_k - y_k)}{|x-y|^5}. \tag{4}$$

The solution of [1] can now be written as:

$$V_k(x) = \int_{\Sigma_1} U_{ki}(x, y)\sigma_{ij}(V, p)n_j \, dy + \int_{\Sigma_3} U_{ki}(x, y)f_i(y) \, dy - \int_{\Sigma_1 \cup \Sigma_3} V_i(y)\sigma_{ij}(U_k, q_k)_y n_j \, dy; \tag{5}$$

n_i is the outward pointing unit normal vector and f_i is the stress difference across the wall Σ_3. The last term on the r.h.s. of [5] vanishes on Σ_3, because V_i is zero there, and vanishes on Σ_1 since on Σ_1, $\mathbf{V} = \mathbf{V}^0$ is a rigid-body motion. One may solve [5] directly [such is the starting point in Yan *et al.* (1987)], but this requires the truncation of the integral on the infinite domain Σ_3. We now describe the Green function method.

The Green function of the Stokes equation for the infinite plane $X_3 = 0$ in the half space $X_3 \geqslant 0$ (Blake 1971) consists of the velocity field G,

$$G_{kl}(x, y) = -\frac{1}{8\pi}\left(\frac{\delta_{ik}}{R} + \frac{R_k R_l}{R^3}\right) + G^1_{ki}(x, y), \tag{6}$$

and the pressure field g,

$$g_k(x, y) = \frac{1}{4\pi}\frac{R_k}{R^3} + g^1_k(x, y), \tag{7}$$

where

$$R_k = y_k - x'_k,$$
$$x'_k = x_k \qquad \text{for } k = 1, 2,$$
$$x'_3 = -x_3$$

and

$$R = |y - x'|.$$

The velocity tensor G^1 is

$$G^1_{kl}(x, y) = (\delta_{k\alpha}\delta_{\alpha j} - \delta_{k3}\delta_{3j})\bar{G}_{jl}(x, y), \qquad \alpha = 1, 2, \tag{8}$$

and

$$\bar{G}_{jl}(x, y) = \frac{x_3}{4\pi}\frac{\partial}{\partial R_j}\left(\frac{x_3 R_l}{R^3} - \frac{\delta_{l3}}{R} - \frac{R_l R_3}{R^3}\right). \tag{9}$$

The pressure vector g^1 is

$$g^1_k(x, y) = (\delta_{k\alpha}\delta_{\alpha j} - \delta_{k3}\delta_{j3})\bar{g}_j(x, y)$$

and

$$\bar{g}_j(x, y) = -\frac{x_3}{2\pi}\frac{\partial}{\partial R_j}\left(\frac{R_3}{R^3}\right). \quad [10]$$

The sum $U_{ik} + G_{ik}$ is the flow field generated by a unit force in the half space $X_3 > 0$ in the presence of a wall at $X_3 = 0$. It can be verified that

$$(U_{ik} + G_{ik})\Big|_{\substack{x_3=0\\ y_3>0}} = (U_{ik} + G_{ik})\Big|_{\substack{y_3=0\\ x_3>0}} = 0. \quad [11]$$

Therefore, the velocity in the half space $z_3 > 0$, generated by the motion of a body above the hole plane ($x_3 > 0$) is given by the expression

$$V_k^+(z) = \int_{\Sigma_1} [U_{ki}(z, x) + G_{ki}(z, x)]\varphi_i(x)\,dx - n_3\int_{\Sigma_2} V_i(y)\sigma_{i3}(U_k + G_k, q_k + g_k)_y\,dy \equiv W_k(z) + W_k^+(z), \quad [12]$$

φ_i is the stress on Σ_1, $n_3 = -1$ on Σ_2 and V_i is the unknown velocity on Σ_2. From [4] it follows that on Σ_2,

$$E_{ik}(z, y) \equiv \sigma_{i3}(U_k, q_k) = \frac{3}{4\pi}\frac{z_3(z_k - y_k)(z_i - y_i)}{|z - x|^5}. \quad [13]$$

A lengthy calculation shows that also, for (G, g),

$$\sigma_{i3}(G_k, g_k)_y = E_{ik}(z, y). \quad [14]$$

Thus,

$$W_k^+(z) = 2\int_{\Sigma_2} E_{ik}(z, y)V_i(y)\,dy. \quad [15]$$

Due to the theorem on the discontinuity of the double-layer potential (see Ladyzhenskaya 1963), we have:

$$\lim_{\substack{z_3\to 0\\ z_3>0}} W_k^+(z) = \begin{cases} V_k(z) & z \in \Sigma_2 \\ 0 & z \in \Sigma_3 \end{cases} \quad [16]$$

and due to [11],

$$\lim_{z_3\to 0} W_k(z) = 0. \quad [17]$$

For the half space $Z_3 < 0$, we define the velocity as

$$V_k^-(z) = -2\int_{\Sigma_2} E_{ik}(z, y)V_i(y)\,dy \quad [18]$$

and again

$$\lim_{\substack{z_3\to 0\\ z_3<0}} V_k^-(z) = \begin{cases} V_k(z) & z \in \Sigma_2 \\ 0 & z \in \Sigma_3 . \end{cases} \quad [19]$$

The velocity **V** is now defined as

$$V_k(z) = \begin{cases} V_k^+(z) & z > 0 \\ V_k^-(z) & z < 0 . \end{cases} \quad [20]$$

Defined in such a way, in terms of the unknown velocity in the hole, the vanishing of the velocity on the wall Σ_3 and the continuity in the hole Σ_2 are automatically fulfilled. Likewise, the pressure can be defined in terms of the single-layer potential for the pressure, the Green function for the pressure and the stress on Σ_1, and twice the double-layer potential for the pressure and the unknown velocity on Σ_2. For $z > 0$, the pressure P^+ is given as the sum $P^+ = P^1 + P^2$, where:

$$P^1(z) = -\int_{\Sigma_1} [q_k(z, x) + g_k(z, x)]\varphi_k(x)\,dx \qquad [21]$$

and

$$P^2(z) = 4\int_{\Sigma_2} \frac{\partial q_i}{\partial y_j} V_i(y) n_j\,dy. \qquad [22]$$

$P^1(z)$ vanishes for $z_3 = 0$; on Σ_2 $n_j = \delta_{j3}$ and $y_3 = 0$. Defining

$$N_i(z, y) = \frac{1}{2\pi}\left(\frac{\delta_{i3}}{|z - y|^3} + 3\frac{z_3(y_i - z_i)}{|z - y|^5}\right), \qquad [23]$$

[22] can now be written as

$$P^2(z) = 2\int_{\Sigma_2} N_i(z, y) V_i(y)\,dy. \qquad [24]$$

Similarly, for $z < 0$

$$P^-(z) = -2\int_{\Sigma_2} N_i(z, y) V_i(y)\,dy. \qquad [25]$$

The two unknowns are the stress φ_i on Σ_1 and the velocity V_i on the hole Σ_2. The first integral equation is obtained by requiring the fulfillment of the boundary conditions on Σ_1, i.e. by letting the field point Z in [12] approach the surface Σ_1 we require:

$$\int_{\Sigma_1} [U_{ki}(z, x) + G_{ki}(z, x)]\varphi_i(x)\,dx + 2\int_{\Sigma_2} E_{ki}(z, y) V_i(y)\,dy = V_k^0, \qquad Z \in \Sigma_1. \qquad [26]$$

The second equation is obtained by requiring the continuity of the normal components of the stress tensor of the flows (V^+, P^+) and (V^-, P^-) in the hole, i.e.

$$\lim_{\substack{z_3 \to 0 \\ z_3 > 0}} \sigma_{i3}(V^+, P^+) = \lim_{\substack{z_3 \to 0 \\ z_3 < 0}} \sigma_{i3}(V^-, P^-). \qquad [27]$$

In the appendix we prove that the continuity of the velocity components in the hole ([16] and [19]) and the above requirements [27] are sufficient conditions for the unique determination of the solution in both sides of the wall–hole plane. The limiting process [27] is not straightforward since the kernel $N_i(z, y)$ in [24] and [25] and the space derivatives of $E_{ik}(z, y)$ in [15] and [18] have singularity $1/|z - y|^3$, which is not integrable on the hole plane. However, this difficulty can be overcome by performing integration by parts, if only V_i is smooth enough. This is described in the next section. By separating the flow (V^+, P^+) according to [12], [21] and [22], we obtain:

$$\int_{\Sigma_1} E_{ij}(x, z)\varphi_j(x)\,dx = -\int_{\Sigma_2} D_{ij}(1/|z - y|) V_j(y)\,dy, \qquad z \in \Sigma_2; \qquad [28]$$

where

$$D_{ij} = \left(\frac{\partial^2}{\partial z_i\,\partial z_j} - \delta_{ij}\frac{\partial^2}{\partial z_3^2} - \delta_{j3}\frac{\partial^2}{\partial z_i\,\partial z_3} - \delta_{i3}\frac{\partial^2}{\partial z_j\,\partial z_3}\right). \qquad [29]$$

Equations [26] and [28] form the system to be solved.

3. DISCRETIZATION OF THE EQUATIONS

Equation [28] cannot be discretized directly due to its strong singularity, however, since $1/|z-y|$ is a harmonic function we have

$$\frac{\partial^2}{\partial z_3^2}\frac{1}{|z-y|} = -\left(\frac{\partial^2}{\partial z_1^2}+\frac{\partial^2}{\partial z_2^2}\right)\frac{1}{|z-y|}.$$

It then follows that:

$$D_{11} = 2\frac{\partial^2}{\partial z_1^2}+\frac{\partial^2}{\partial z_2^2}; \qquad D_{22} = \frac{\partial^2}{\partial z_1^2}+2\frac{\partial^2}{\partial z_2^2}; \qquad D_{12} = D_{21} = \frac{\partial^2}{\partial z_1\,\partial z_2};$$

$$D_{33} = 2\left(\frac{\partial^2}{\partial z_1^2}+\frac{\partial^2}{\partial z_2^2}\right); \qquad D_{i3} = 0 \quad \text{for } i \neq 3; \qquad D_{3j} = 0 \quad \text{for } j \neq 3.$$

D_{ij} is a symmetric operator.

The analytical solution for the field generated by a point force, located above a circular hole (Davis *et al.* 1981), shows that both the vertical and horizontal components of the fluid velocity in the hole vanish on the edge of the hole. We divide the hole into triangles and an approximation for the velocity is sought in terms of linear base functions that vanish on the edge, see figure 2. For each triangle vertex, which is not on the edge, a linear function $h(y)$ is defined such that it equals 1 on this vertex and zero on all the other. Such functions are continuous throughout the hole, vanish on the edge and have piecewise continuous first-order derivatives. In order to reduce the singularity of [28], the Galerkin method is used with the same base functions. Two integrations by parts are performed, the singularity is reduced to $1/|z-y|$ and the symmetry of D_{ij} is preserved. This integrable singularity is eliminated by transforming the double surface integral to a double path integral. The matrix form of the r.h.s. of [28], $\tilde{D}$, consists of submatrices $\tilde{M}(k,l)_{ij}$, of order 3×3, representing the interaction between the kth and the lth vertices and having the following form:

$$\tilde{M}_{11}(k,l) = \frac{1}{2\pi}\sum_m\sum_n (2A_m^k A_n^l + B_m^k B_n^l) I_{mn}, \qquad [30a]$$

$$\tilde{M}_{22}(k,l) = \frac{1}{2\pi}\sum_m\sum_n (A_m^k A_n^l + 2B_m^k B_n^l) I_{mn}, \qquad [30b]$$

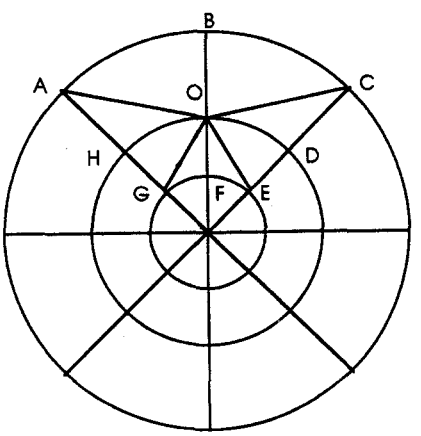

Figure 2. An element in the hole, corresponding to the node 0.

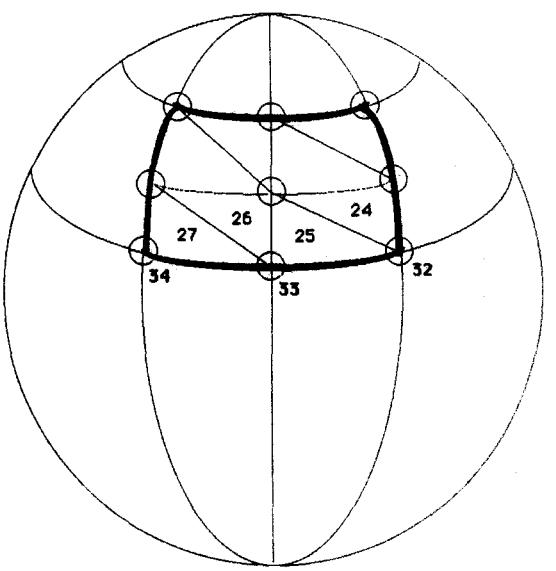

Figure 3. An element on the surface of the body, composed of several triangles.

$$\tilde{M}_{12}(k,l) = \tilde{M}_{21}(k,l) = \frac{1}{2\pi} \sum_m \sum_n A_m^k B_n^l I_{mn} \qquad [30c]$$

and

$$\tilde{M}_{33}(k,l) = \frac{1}{\pi} \sum_m \sum_n (A_m^k A_n^l + B_m^k B_n^l) I_{mn}. \qquad [30d]$$

The summation is taken over all triangles m containing the vertex k, and all triangles n containing the vertex l;

$$I_{mn} \equiv \int_{L_m} \int_{L_n} (|z-y|\, dz_1\, dy_1 + |z-y|\, dz_2\, dy_2). \qquad [31]$$

The integration is performed over the circumference of the mth and nth triangles. A_m^k, B_m^k and C_m^k are the coefficients defining the kth base function on the mth triangle:

$$h^k(y) = A_m^k y_1 + B_m^k y_2 + C_m^k.$$

The surface of the body is divided into elements, each of which consists of several flat triangles which have their vertices on the actual surface of the body, see figure 3. The elements are therefore not planar. The base functions are taken to be constant on each element. Though, perhaps, not the best approximation for a sphere, this method is easily applied to non-regular geometries, especially if the surface of a body is given in terms of a finite number of points. The surface of the sphere was divided into 396 triangles, comprising 108 elements.

Numerical calculations for this approximated sphere in an unbounded fluid yielded an error or 1.5% for the forces and 4.5% for the torques. In the following, we shall compare numerical results with the above computed results for the approximated surface. The Galerkin method is used in [26] with the constant base functions. After integration, [26] and [28] assume the following form:

$$\left.\begin{aligned} [\tilde{U} + \tilde{G}) \cdot \varphi + 2 \cdot \tilde{E} \cdot v &= V^0 \\ \tilde{E}^t \cdot \varphi + \tilde{D} \cdot v &= 0. \end{aligned}\right\} \qquad [32]$$

$\tilde{U} + \tilde{G}$ and $\tilde{D}$ are symmetric and positive definite matrices. $\tilde{D}$ is well-conditioned, having a condition number of about 10. $\tilde{D}$ depends, of course, on the arrangement of the elements composing the hole. Due to its well-conditioning, matrix $\tilde{D}$ is easily inverted and system [32] is reduced to a single equation:

$$[\tilde{U} + \tilde{G} - 2 \cdot \tilde{E} \cdot \tilde{D}^{-1} \cdot \tilde{E}^t] \cdot \varphi = V^0. \qquad [33]$$

This matrix is symmetric and positive definite, its dimension is $N \times 3$, N being the number of elements on the surface of the body. Equation [33] with $\tilde{U}$ only corresponds to the case of a particle in an unbounded fluid, and with $\tilde{U}$ and $\tilde{G}$ to the case of an infinite plane wall. The term $\tilde{E} \cdot \tilde{D}^{-1} \cdot \tilde{E}$ decreases fast as the particle moves away from the hole.

4. RESULTS

Computations were performed for a circular hole of radius $R = 1$, for approximated spherical bodies of radii $R = 0.1$, 0.5, 1 and 5, and for an approximated ellipsoid of axes A = B = 0.5 and C = 1, and A = B = 0.25 and C = 0.5. In the following, results will be presented for the translation, coupling and rotation tensors **K**, **C** and **T**. **K** and **T** are symmetric and negative definite. K_{ij} is the ith component of the force acting on a body moving in the jth direction with unit velocity. T_{ij} is the torque due to unit angular velocity. C_{ij} is the jth component of the force due to rotation in the ith direction and the ith component of the torque due to translation in the jth direction; it is, in general, not symmetric.

In table 1 we show a comparison of results of computations with different sets of elements which compose the hole. For all six points of calculation the value of $-K_{zz}$ is a monotonic decreasing function of the number of elements. Since the differences between cases c and d were not large, we decided to perform all the calculations with the set c, i.e. with 192 elements. For the approximation of the surface of the particles, spheres and ellipsoids, we used 108 elements composed of 396 triangles. The accuracy of the calculations depends, among other things, on the

Table 1. Convergence of $-K_{zz}/|K_{zz}^{\infty}|$; sphere $R = 0.5$, $Z/R = 1.1$

No. of elements[a]	X					
	0	0.2	0.4	0.6	0.8	1
(a)	1.4841	1.5195	1.6623	2.0553	3.4202	6.9929
(b)	1.4741	1.5703	1.6400	1.9892	3.0329	6.2325
(c)	1.4724	1.5055	1.6365	1.9750	3.0027	6.2264
(d)	1.4702	1.5055	1.6359	1.9744	2.9989	6.1987

[a]Number of elements in hole: (a)—96, (b)—128, (c)—192, (d)—224.

size and distance of the elements in the hole relative to the size of the particle. Therefore, because of the high singularity of the operator E as the body approaches the hole, some of the singular terms are calculated via a semi-analytic method. Different calculation times were therefore needed for different locations and orientations of the particles. Calculations were performed on a CDC computer Cyber 180/855. The time needed for the calculation of the three resistance tensors **K**, **C** and **T** for the sphere was 150–170 CPU s. In table 2, a comparison is made for the axisymmetric case (a sphere is located along the hole's symmetry axis and moves vertically) with previous results. The numerical values are the ratio $-K_{zz}/|K_{zz}^{\infty}|$, K_{zz}^{∞} is the value for an unbounded fluid. We have used for the "approximated" body the value $K_{zz}^{\infty} = -18.576 \cdot R$, calculated by our method, which differs from the perfect sphere value of $6\pi R$ by 1.5%. Results are given for different sphere radii R and for different Z/R ratios, Z being the distance of the sphere's center from the plane. The values for $R = 0.5$ are shown in figure 4 and for $R = 0.1$ in figure 5. Calculations for $R = 0.1$ were performed with small elements near the center of the hole, whereas in the other cases the areas of the elements were more or less equal. This explains the better results obtained in this case. In table 3, results are given for $-K_{zz}/|K_{zz}^{\infty}|$, for $R = 0.5$ and for the center of the body located at distances X from the hole's symmetry axis. Comparison is made with the results of Yan *et al.* (1987); however, since their results are given on a graph, the values could not be discerned accurately. The right-hand column shows the ratio for the wall effect K_{zz}^{w} with no hole, as calculated from [33] when the matrix $2 \cdot \tilde{E} \cdot \tilde{D}^{-1} \cdot \tilde{E}^{t}$ is omitted. These results are compared with the analytical results of Happel & Brenner (1973). For $Z/R = 1.1$ the difference between our results and Yan *et al.* (1987) is 5.5%, and the difference between our results and the theoretical results in the absence of the wall is 4.4%. These results are presented in figure 6. The rise in the force occurs mainly near the edge in the range $0.8 < x < 1.2$.

In table 4 we present results for $K_{xz}/|K_{zz}^{\infty}|$. Since all the terms are positive, a particle which moves parallel to the wall towards the center of the hole experiences a force directed towards the wall. If it moves towards the hole plane it experiences a force directed towards the center of the hole. Our results are up to one order of magnitude higher than the results of Yan *et al.* (1987). Results of the same order of magnitude were obtained for ellipsoids. The difference in results may stem from the small number of spherical harmonics, only four, used by Yan *et al.* to satisfy the

Table 2. Axisymmetric case $-K_{zz}/|K_{zz}^{\infty}|$; sphere.

Z/R	Ref.[a]	R			
		0.1	0.5	1	5
10	(a)	1.0738	1.1229	1.1240	1.1242
	(b)	1.0596	1.1240	1.1262	1.1262
	(c)	1.0723	1.1246	1.1259	1.1261
5	(a)	1.0679	1.2590	1.2768	1.2800
	(b)	1.0532	1.2509	1.2795	1.2850
	(c)	1.0666	1.2618	1.2804	1.2837
2	(a)	1.0553	1.4866	1.8710	2.0952
	(b)	1.0505	1.3919	1.8058	2.1200
	(c)	1.0540	1.4264	1.8654	2.1194
1.5	(a)	1.0554	1.4938	2.1715	3.1059
	(b)	1.0504	1.3882	2.0334	3.1535
	(c)	1.0523	1.4205	2.1042	3.1530
1.1	(a)	1.0558	1.4724	2.4893	8.3893
	(b)	1.0503	1.3777	2.2867	8.9400
	(c)	1.0513	1.3946	2.3600	8.4700

[a](a) Present work; (b) Dagan *et al.* (1982b); (c) Yan *et al.* (1987).

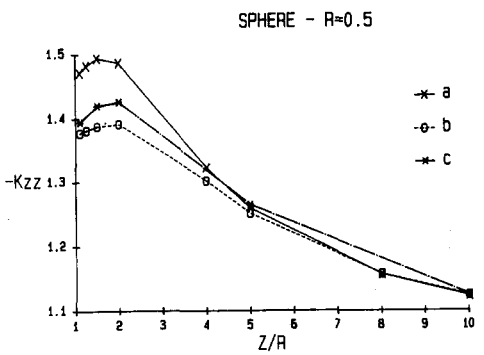

Figure 4. The axisymmetric case. (a) Present work; (b) Dagan *et al.* (1982b); (c) Yan *et al.* (1987).

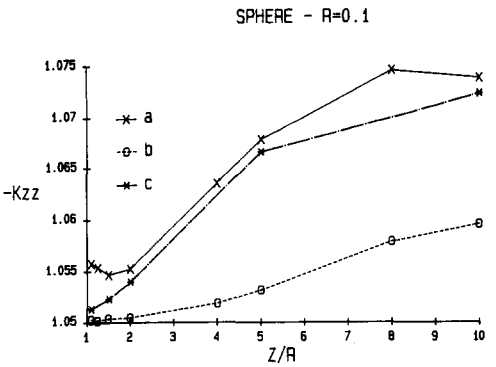

Figure 5. The axisymmetric case. (a) Present work; (b) Dagan *et al.* (1982b); (c) Yan *et al.* (1987).

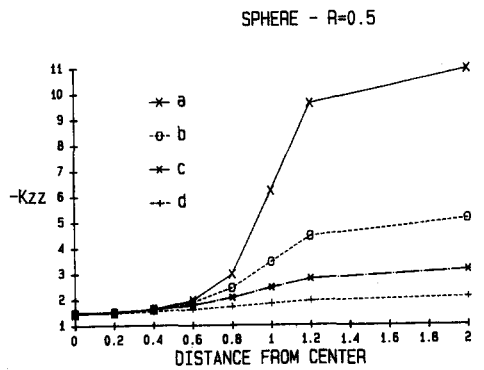

Figure 6. $-K_{zz}$ vs the distance from the center. (a) $Z/R = 1.1$; (b) $Z/R = 1.25$; (c) $Z/R = 1.5$; (d) $Z/R = 2$.

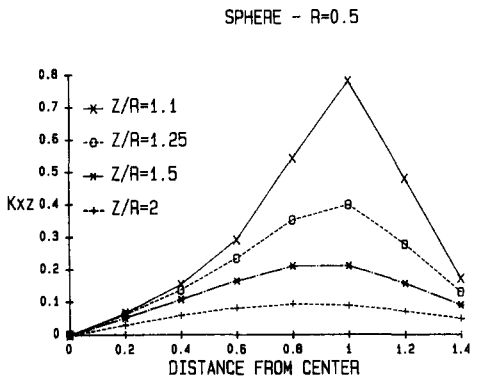

Figure 7. The transverse force, $K_{xz}/|K_{zz}^{\infty}|$.

Table 3. $-K_{zz}/|K_{zz}^{\infty}|$; sphere $R = 0.5$.

		X					
Z/R	Ref.[a]	0	0.5	0.75	1	2	∞
10	(a)	1.123	1.123	1.123	1.123	1.123	1.124
	(b)	1.125	1.100	1.100	1.100	1.100	1.126
4	(a)	1.322	1.329	1.336	1.344	1.367	1.373
	(b)	1.30	1.300	1.300	1.300	—	1.380
2	(a)	1.487	1.585	1.705	1.848	2.089	2.099
	(b)	1.426	1.450	1.550	1.650	—	2.126
1.5	(a)	1.494	1.682	1.985	2.449	3.125	3.139
	(b)	1.421	1.600	1.900	2.500	—	3.205
1.1	(a)	1.472	1.766	2.606	6.226	10.921	10.928
	(b)	1.3946	1.700	2.600	—	—	11.459

Z—distance from the wall plane, X—distance from the hole center.
[a](a) Present work; (b) Yan *et al.* (1987), right-hand column—analytical.

Table 4. Transverse force $K_{xz}/|K_{zz}^{\infty}|$; sphere $R = 0.5$

		X							
Z/R	Ref.[a]	0	0.2	0.4	0.6	0.8	1	1.2	1.4
2	(a)	0	0.0314	0.0606	0.0838	0.0951	0.0904	0.0722	0.0497
	(b)	0	0.0150	0.0200	0.0300	0.0350	0.0300	0.0200	0.0200
1.5	(a)	0	0.0524	0.1082	0.1661	0.2115	0.2118	0.1569	0.0899
	(b)	0	0.0300	0.0500	0.0600	0.0600	0.0500	0.0400	0.0300
1.25	(a)	0	0.0632	0.1384	0.2365	0.3535	0.4000	0.2781	0.1306
	(b)	—	—	—	—	—	—	—	—
1.1	(a)	0	0.0679	0.1562	0.2940	0.5446	0.7823	0.4807	0.1732
	(b)	0	0.0400	0.0700	0.0800	0.0800	0.0600	0.0500	0.0400

[a](a) Present work; (b) Yan *et al.* (1987).

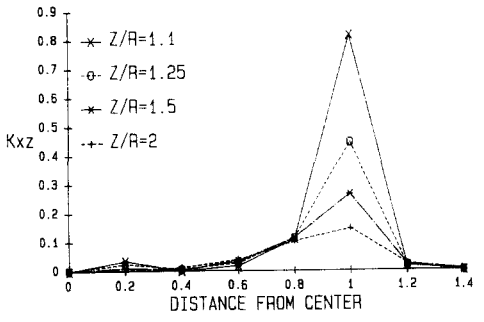

Figure 8. The transverse force, $K_{xz}/|K_{zz}^{\infty}|$.

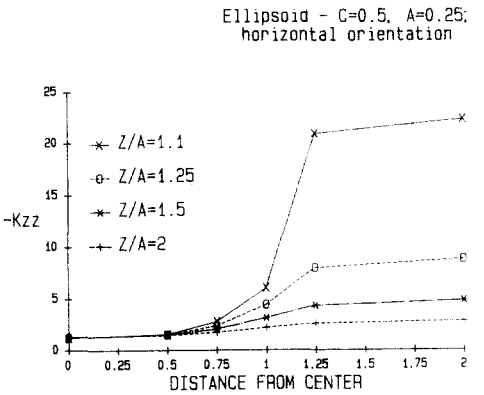

Figure 9. $-K_{zz}/|K_{zz}^{\infty}|$; ellipsoid $\Theta = \pi/2$.

boundary conditions on the surface of the sphere. Such a small number, which is enough for the other terms, may prove to be insufficient for the transverse components. This component of the force is important for the collection efficiency of the hole. A particle which moves towards the hole in a quiet fluid will experience a considerable additional force directed towards the wall. If, on the other hand, the particle is immersed in a flow and lags after it due to its inertia, this additional force will be directed away from the wall, thus decreasing the collection efficiency. This phenomenon was reported by Dagan *et al.* (1983). The results for spheres of radii $R = 0.1$ and $R = 0.5$ are shown in figures 7 and 8. The domain of significance for $R = 0.1$ is much narrower than for $R = 0.5$. Large differences also occur in the values for C_{yz}; given in table 5.

We now present results for elongated ellipsoids. Let Θ be the angle which the symmetry axis of the ellipsoid forms with the X_3 axis when rotated about the X_2 axis. The values of the resistance tensors, calculated by our numerical method for an unbounded fluid and an ellipsoid with axes C = 1 and A = 0.5 are $K_{zz}^{\infty} = -11.182$ and $K_{xx}^{\infty} = -12.775$ for $\Theta = 0$. For $\Theta = \pi/2$ these values are interchanged. The analytical values are $K_{zz}^{\infty} = -11.347$ and $K_{xx}^{\infty} = -12.996$, a difference of 1.7%. Our value for the rotation term $T_{yy}^{\infty} = -8.9312$ is 5.5% smaller than the analytical value (Happel & Brenner 1973). In table 6 numerical tests are shown, with different sets of elements in the hole, for ellipsoids of axes C = 1 and A = 0.5, $\Theta = 0$ and $\pi/2$. As in table 1, the values decrease as the number of elements increases. Again we decided to use the same set of 192 elements as before. The

Table 5. Coupled force $C_{yz}/|K_{zz}^{\infty}| \cdot R$; sphere $R = 0.5$

		X							
Z/R	Ref.[a]	0	0.2	0.4	0.6	0.8	1	1.2	1.4
2	(a)	0	0.006	0.013	0.018	0.021	0.020	0.017	0.012
	(b)	0	0.000	0.006	0.010	0.010	0.010	0.006	0.004
1.5	(a)	0	0.015	0.031	0.049	0.065	0.068	0.050	0.028
	(b)	0	0.000	0.010	0.020	0.040	0.040	—	—
1.25	(a)	0	0.023	0.049	0.087	0.139	0.167	0.1125	0.050
	(b)	—	—	—	—	—	—	—	—
1.1	(a)	0	0.029	0.065	0.126	0.256	0.438	0.238	0.076
	(b)	0	0.005	0.015	0.040	0.080	0.120	—	—

[a](a) Present work; (b) Yan *et al.* (1987).

Table 6. Convergence of $-K_{zz}/|K_{zz}^{\infty}|$; ellipsoid A = 0.5 and C = 1

		X				
Θ	No. of elements[a]	0	0.5	0.75	1	2
0	(a)	1.5766	1.7293	2.0263	2.7366	3.5895
0	(b)	1.5758	1.7270	2.0193	2.7260	3.5894
0	(c)	1.5757	1.7268	2.0191	2.7257	3.5894
$\pi/2$	(a)	2.0003	3.0319	4.5102	6.1833	22.3643
$\pi/2$	(b)	1.9957	3.0046	4.4970	6.1112	22.3632
$\pi/2$	(c)	1.9954	3.0041	4.4956	6.1022	22.3630

[a]Number of elements in hole: (a) – 128, (b) – 192, (c) – 224.

time of calculation varied from 400 to 500 CPU s. In table 7 we present results for C = 1, A = 0.5 and $\Theta = \pi/2$. The same results for $\Theta = 0$ are shown in table 8. The same sets of results for C = 0.5 and A = 0.25 are shown in figures 9–11. In table 9 results are shown for C = 0.5 and A = 0.25 for the transverse and the coupled force. The transverse force is normalized by $K^{\infty} = \frac{1}{2}[K^{\infty}_{xx} + K^{\infty}_{zz}]$. The coupled force C_{yz} is normalized by $\sqrt{|K^{\infty}_{zz} \cdot T^{\infty}_{yy}|}$ to make it dimensionless. These results are presented also in figures 12 and 13. One should note the similarity between these two graphs and also their similarity to the transverse force on a sphere, figure 7. The same results but for $\Theta = 0$ are given in table 10 and in figures 14 and 15. The dependence of the force on the distance from the center is similar for $\Theta = \pi/2$ and $\Theta = 0$ but the magnitude in the last case is smaller, since in the horizontal orientation the center of the body is closer to the wall than in the vertical orientation. An interesting difference between the two orientations occurs in the sign of C_{yz}. Ellipsoids with

Table 7. Ellipsoid C = 1, A = 0.5 and $\Theta = \pi/2$

		X							
Z/A	Force[a]	0	0.5	0.75	1	1.25	2	3	∞
2	(a)	1.8522	1.9926	2.1493	2.3360	2.5194	2.8105	2.8496	2.8511
	(b)	1.4314	1.4279	1.4250	2.4231	1.4240	1.4461	1.4636	1.4666
	(c)	1.1636	1.1749	1.1832	1.1918	1.2036	1.2494	1.2617	1.2622
1.5	(a)	1.9385	2.2892	2.7047	3.2615	3.9168	4.7665	4.8213	4.8223
	(b)	1.5805	1.5913	1.6011	1.6127	1.6246	1.6852	1.7139	1.7167
	(c)	1.2319	1.2898	1.3270	1.3510	1.3809	1.5271	1.5499	1.5504
1.25	(a)	1.9757	2.6123	3.4156	4.5261	6.7045	8.7585	8.8242	8.8249
	(b)	1.6898	1.7354	1.7757	1.8272	1.8680	1.9831	2.0200	2.0223
	(c)	1.2823	1.4325	1.5370	1.5792	1.6271	1.9466	1.9785	1.9790
1.1	(a)	1.9957	3.0046	4.4970	6.1112	16.0313	22.3632	22.4360	22.4362
	(b)	1.7715	1.8722	1.9670	2.1096	2.2301	2.4264	2.4697	2.4721
	(c)	1.3201	1.6116	1.8724	1.9348	2.0051	2.6175	2.6572	2.6577

[a](a) $-K_{zz}/|K^{\infty}_{zz}|$; (b) $-K_{xx}/|K^{\infty}_{xx}|$; (c) $-T_{yy}/|T^{\infty}_{yy}|$.

Table 8. Ellipsoid C = 1, A = 0.5 and $\Theta = 0$

		X							
Z/C	Force[a]	0	0.5	0.75	1	1.25	2	3	∞
2	(a)	1.4311	1.4463	1.4624	1.4803	1.4965	1.5322	1.5309	1.5322
	(b)	1.2582	1.2562	1.2545	1.2530	1.2525	1.2555	1.2595	1.2616
	(c)	1.0584	1.0583	1.0583	1.0584	1.0587	1.0598	1.0577	1.0602
1.5	(a)	1.5271	1.5855	1.6561	1.7391	1.8086	1.8845	1.8949	1.8956
	(b)	1.3657	1.3640	1.3613	1.3591	1.3611	1.3782	1.3870	1.3895
	(c)	1.0759	1.0787	1.0809	1.0827	1.0851	1.0896	1.0902	1.0902
1.25	(a)	1.5634	1.6726	1.8373	2.0832	2.2872	2.4327	2.4440	2.4432
	(b)	1.4540	1.4631	1.4691	1.4701	1.4814	1.5225	1.5345	1.5369
	(c)	1.0921	1.1039	1.1161	1.1260	1.1343	1.1440	1.1445	1.1446
1.1	(a)	1.5758	1.7270	2.0193	2.7260	3.3463	3.5894	3.6007	3.5924
	(b)	1.5220	1.5517	1.5885	1.6165	1.6508	1.7254	1.7394	1.7416
	(c)	1.1043	1.1292	1.1672	1.2105	1.2362	1.2524	1.2529	1.2532

[a](a) $-K_{zz}/|K^{\infty}_{zz}|$; (b) $-K_{xx}/|K^{\infty}_{xx}|$; (c) $-T_{yy}/|T^{\infty}_{yy}|$.

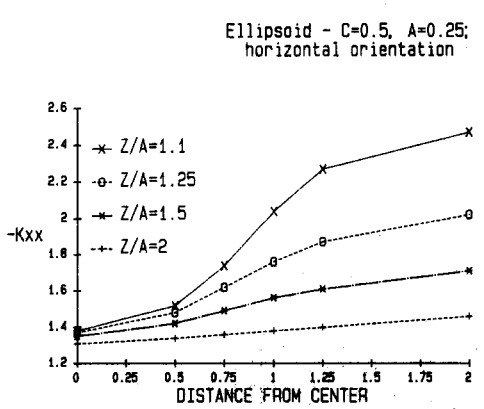

Figure 10. $-K_{xx}/|K^{\infty}_{xx}|$; ellipsoid $\Theta = \pi/2$.

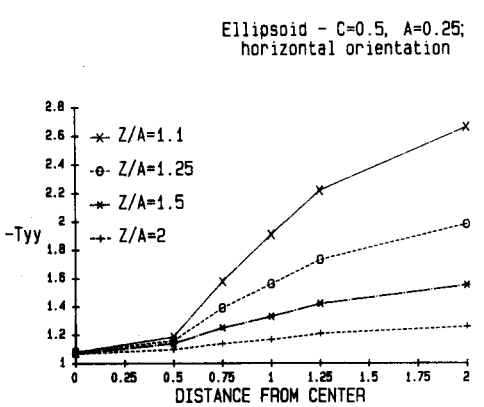

Figure 11. $-T_{yy}/|T^{\infty}_{yy}|$; ellipsoid $\Theta = \pi/2$.

Table 9. Ellipsoid C = 0.5, A = 0.25 and $\Theta = \pi/2$

		X					
Z/A	Force[a]	0	0.5	0.75	1	1.25	2
2	(a)	0	0.1153	0.1727	0.1778	0.1138	0.00
	(b)	0	0.0951	0.1698	0.1853	0.1063	0.00
1.5	(a)	0	0.1500	0.2755	0.3280	0.1996	0.00
	(b)	0	0.1382	0.3393	0.4436	0.2382	0.00
1.25	(a)	0	0.1688	0.3780	0.5120	0.3063	0.00
	(b)	0	0.1669	0.5531	0.8395	0.4340	0.00
1.1	(a)	0	0.1800	0.4919	0.7314	0.4509	0.00
	(b)	0	0.1871	0.8242	1.4370	0.7574	0.00

(a) $K_{xz}/|K^{\infty}|$; (b) $C_{yz}/\sqrt{|K_{zz}^{\infty} \cdot T_{yy}^{\infty}|}$. $K^{\infty} = \frac{1}{2}[K_{xx}^{\infty} + K_{zz}^{\infty}]$.

Table 10. Ellipsoid C = 0.5, A = 0.25 and $\Theta = 0$

		X					
Z/C	Force[a]	0	0.5	0.75	1	1.25	2
2	(a)	0	0.0412	0.0525	0.0483	0.0323	0.00
	(b)	0	−0.0105	−0.0144	−0.0125	−0.0000	−0.00
1.5	(a)	0	0.0709	0.1066	0.1046	0.0553	0.00
	(b)	0	−0.0144	−0.0288	−0.0297	−0.0096	−0.00
1.25	(a)	0	0.0872	0.1557	0.1830	0.0744	0.00
	(b)	0	−0.0120	−0.0391	−0.0573	−0.0108	−0.00
1.1	(a)	0	0.0948	0.1941	0.3163	0.0900	0.00
	(b)	0	−0.0072	−0.0427	−0.1127	−0.0105	−0.00

[a](a) $K_{xz}/|K^{\infty}|$; (b) $C_{yz}/\sqrt{|K_{zz}^{\infty} \cdot T_{yy}^{\infty}|}$. $K^{\infty} = \frac{1}{2}[K_{xx}^{\infty} + K_{zz}^{\infty}]$.

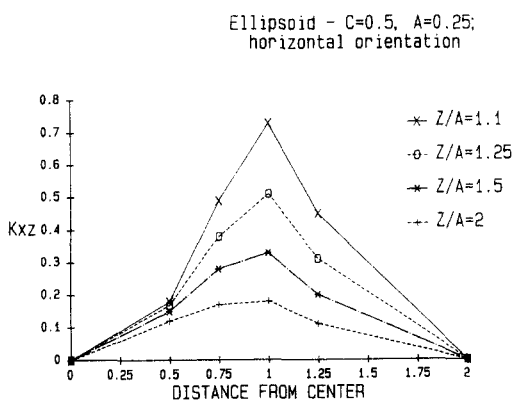

Figure 12. $K_{zz}/|K^{\infty}|$; ellipsoid $\Theta = \pi/2$, $K^{\infty} = \frac{1}{2}[K_{xx}^{\infty} + K_{zz}^{\infty}]$.

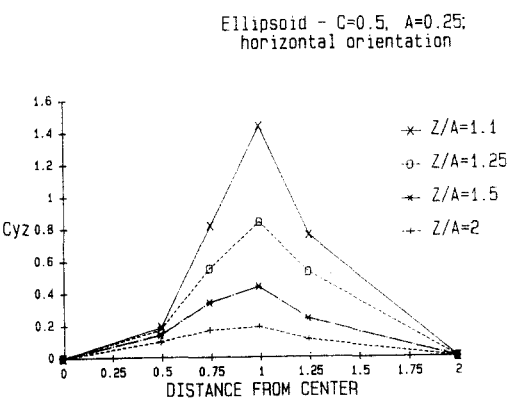

Figure 13. $C_{yz}/\sqrt{|K_{zz}^{\infty} \cdot T_{yy}^{\infty}|}$, ellipsoid $\Theta = \pi/2$.

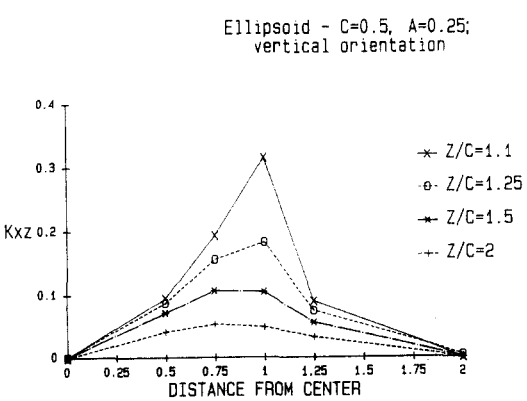

Figure 14. $K_{xz}/|K^{\infty}|$; ellipsoid $\Theta = 0$, $K^{\infty} = \frac{1}{2}[K_{xx}^{\infty} + K_{zz}^{\infty}]$.

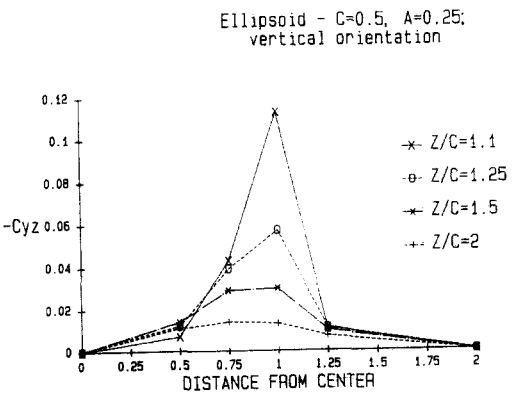

Figure 15. $C_{yz}/\sqrt{|K_{zz}^{\infty} \cdot T_{yy}^{\infty}|}$, ellipsoid $\Theta = 0$.

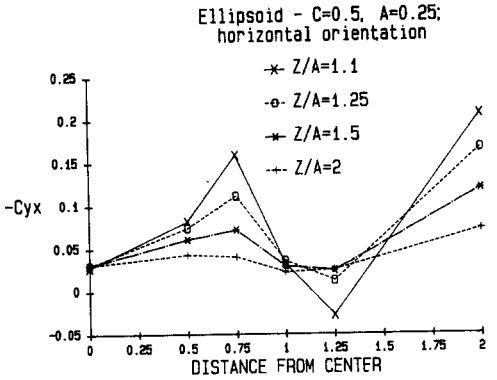

Figure 16. $-C_{yx}/\sqrt{|K_{xx}^{\infty} \cdot T_{yy}^{\infty}|}$, ellipsoid $\Theta = \pi/2$.

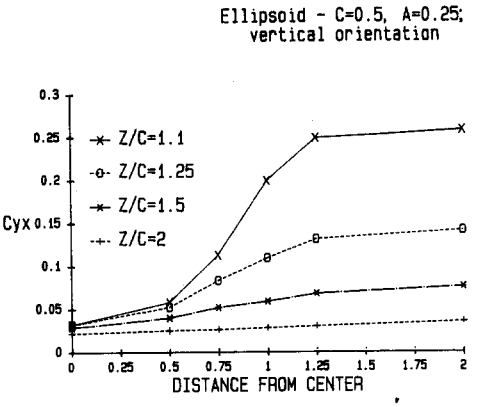

Figure 17. $C_{yx}/\sqrt{|K_{xx}^{\infty} \cdot T_{yy}^{\infty}|}$, ellipsoid $\Theta = 0$.

$\Theta = 0$, approaching the hole, will rotate clockwise in the direction of increasing Θ, whereas those with $\Theta = \pi/2$ will rotate in the direction of decreasing Θ. In tables 11 and 12 we present the same results as in tables 9 and 10 but for C = 1 and A = 0.5. In table 13 the coupled force and torque $C_{yx}/\sqrt{|K_{xx}^{\infty}, T_{yy}^{\infty}|}$ is shown for C = 1, A = 0.5 and C = 0.5, A = 0.25 for $\Theta = 0$ and $\Theta = \pi/2$. The sign of C_{yx} is opposite to that of C_{yz} and its magnitude is smaller. For $\Theta = 0$, C_{yx} is monotonically increasing with the distance from the center but for $\Theta = \pi/2$ the behavior is quite complex and at $x = 1.25$ it even changes sign. In the range $0 \leqslant x \leqslant 1$, fluid, which is pushed down the hole, drags the back side of the particle downwards, whereas fluid which is pushed along the wall drags the front part of the particle upwards. Around $x = 1.25$, more fluid is pushed from the hole forward than downward so that the sign of the torque changes. Finally, for $x > 1.25$, the influence of the hole diminishes, only the influence of the infinite wall is felt and C_{yx} is again negative. It is interesting to note that in the case of a sphere C_{yx} and C_{yz} are both positive. Thus, far from the hole, a sphere and an ellipsoid at $\Theta = 0$, moving in the positive direction of the X-axis, will rotate in the direction of increasing Θ, whereas an ellipsoid at $\Theta = \pi/2$ will rotate in the direction of decreasing Θ.

Table 11. Ellipsoid C = 1, A = 0.5 and $\Theta = \pi/2$

		X					
Z/A	Force[a]	0	0.5	0.75	1	1.25	2
2	(a)	0	0.0890	0.1133	0.1180	0.1030	0.0279
	(b)	0	0.1104	0.1404	0.1431	0.1197	0.0222
1.5	(a)	0	0.1852	0.2427	0.2645	0.2326	0.0403
	(b)	0	0.2720	0.3715	0.3951	0.3361	0.0353
1.25	(a)	0	0.2881	0.3846	0.4486	0.4189	0.0491
	(b)	0	0.4808	0.7218	0.7839	0.7093	0.0456
1.1	(a)	0	0.4011	0.5488	0.6633	0.7695	0.0554
	(b)	0	0.7423	1.2917	1.3700	1.3764	0.0537

[a](a) $K_{xz}/|K^{\infty}|$; (b) $C_{yz}/\sqrt{|K_{zz}^{\infty} \cdot T_{yy}^{\infty}|}$. $K^{\infty} = \frac{1}{2}[K_{xx}^{\infty} + K_{zz}^{\infty}]$.

Table 12. Ellipsoid C = 1, A = 0.5 and $\Theta = 0$

		X					
Z/C	Force[a]	0	0.5	0.75	1	1.25	2
2	(a)	0	0.0150	0.0188	0.0193	0.0171	0.000
	(b)	0	−0.0063	−0.0077	−0.0074	−0.0060	−0.000
1.5	(a)	0	0.0493	0.0630	0.0614	0.0471	0.011
	(b)	0	−0.0206	−0.0265	−0.0245	−0.0162	−0.000
1.25	(a)	0	0.0902	0.1293	0.1326	0.0884	0.013
	(b)	0	−0.0342	−0.0531	−0.0542	−0.0297	−0.000
1.1	(a)	0	0.1251	0.2117	0.2633	0.1438	0.014
	(b)	0	−0.0338	−0.0689	−0.0948	−0.0396	−0.000

[a](a) $K_{xz}/|K^{\infty}|$; (b) $C_{yz}/\sqrt{|K_{zz}^{\infty} \cdot T_{yy}^{\infty}|}$. $K^{\infty} = \frac{1}{2}[K_{xx}^{\infty} + K_{zz}^{\infty}]$.

Table 13. $C_{yx}/\sqrt{|K_{xx}^{\infty} \cdot T_{yy}^{\infty}|}$ for an ellipsoid. $R = C$ for $\Theta = 0$; $R = A$ for $\Theta = \pi/2$

		X							
Z/R	C, A, Θ[a]	0	0.5	0.75	1	1.25	2	3	∞
2	(a)	0.0326	0.0320	0.0316	0.0314	0.0315	0.0334	0.0345	0.0346
	(b)	−0.0752	−0.0645	−0.0532	−0.0428	−0.0381	−0.0594	−0.0733	−0.0746
	(c)	0.0222	0.0249	0.0264	0.0276	0.0300	0.0348	0.0348	0.0346
	(d)	−0.0313	−0.0432	−0.0401	−0.0224	−0.0248	−0.0719	−0.0744	−0.0746
1.5	(a)	0.0600	0.0616	0.0625	0.0633	0.0658	0.0739	0.0755	0.0753
	(b)	−0.1129	−0.1000	−0.0768	−0.0508	−0.0352	−0.0960	−0.1203	−0.1214
	(c)	0.0289	0.0404	0.0520	0.0589	0.0681	0.0761	0.0755	0.0753
	(d)	−0.0314	−0.0612	−0.0716	−0.0285	−0.0241	−0.1191	−0.1214	−0.1214
1.25	(a)	0.0834	0.0950	0.1054	0.1123	0.1213	0.1387	0.1398	0.1394
	(b)	−0.1396	−0.1398	−0.1176	−0.0565	−0.0205	−0.1344	−0.1672	−0.1682
	(c)	0.0315	0.0516	0.0825	0.1088	0.1311	0.1407	0.1396	0.1394
	(d)	−0.0298	−0.0736	−0.1111	−0.0351	−0.0120	−0.1662	−0.1682	−0.1682
1.1	(a)	0.1002	0.1275	0.1648	0.2007	0.2275	0.2569	0.2573	0.2569
	(b)	0.1582	−0.1858	−0.1429	−0.0525	0.0210	−0.1659	−0.2056	−0.2065
	(c)	0.0321	0.0582	0.1134	0.1988	0.2485	0.2583	0.2570	0.2569
	(d)	−0.0283	−0.0819	−0.1596	−0.0323	−0.0282	−0.2047	−0.2066	−0.2065

[a](a) C = 1, A = 0.5, $\Theta = 0$; (b) C = 1, A = 0.5, $\Theta = \pi/2$; (c) C = 0.5, A = 0.25, $\Theta = 0$; (d) C = 0.5, A = 0.25, $\Theta = \pi/2$.

5. CONCLUSION

The boundary element method has been applied to a problem, to date treated by analytical or mixed analytical–numerical methods for spherical bodies only. Results, obtained for these cases, except for the transverse forces, are in good agreement with previous results, though no symmetry assumptions were made. Large differences occurred in the transverse components of the force which, we believe, are due to the method used in previous studies. New results are presented for the first time for ellipsoids and are, in fact, available for any desired geometry of the body and the hole. Moreover, though not applied here, the method can treat more than one hole without requiring additional disc memory, since the order of the "body–hole" interaction matrix is determined only by the number of elements on the body's surface.

Acknowledgement—The author is indebted to the late Professor I. Gallily of the Department of Atmospheric Sciences of the Hebrew University of Jerusalem for suggesting the problem and for fruitful discussions.

REFERENCES

BLAKE, J. R. 1971 A note on the image system for a stokeslet in a no-slip boundary. *Proc. Camb. phil. Soc.* **70,** 303–310.

DAGAN, Z., WEINBAUM, S. & PFEFFER, R. 1982a An infinite-series solution for the creeping motion through an orifice of finite length. *J. Fluid Mech.* **115,** 505–523.

DAGAN, Z., WEINBAUM, S. & PFEFFER, R. 1982b General theory for the creeping motion of a finite sphere along the axis of a circular orifice. *J. Fluid Mech.* **117,** 143–170.

DAGAN, Z., WEINBAUM, S. & PFEFFER, R. 1983 Theory and experiment of the three-dimensional motion of a freely suspended spherical particle at the entrance to a pore at low Reynolds number. *Chem. Engng Sci.* **38,** 583–596.

DAGAN, Z., YAN, Z. Y. & SHEN, H. 1988 The axisymmetric rise of a spherical bubble at the exit of an orifice in the presence of a stagnant cap of insoluble surfactants. *J. Fluid Mech.* **190,** 299–319.

DAVIS, A. M. J. 1983 Force and torque formulae for a sphere moving in an axisymmetric Stokes flow with finite boundaries: asymmetric stokeslets near a hole in a plane wall. *Int. J. Multiphase Flow* **9,** 575–608.

DAVIS, A. M. J., O'NEIL, M. E. & BRENNER, H. 1981 Axisymmetric Stokes flows due to a rotlet or a stokeslet near a hole in a plane wall: filtration flows. *J. Fluid Mech.* **103,** 183–205; **111,** 499–500 (corrigendum).

GANATOS, P., PFEFFER, R. & WEINBAUM, S. 1980 A strong interaction theory of the creeping motion of a sphere between plane parallel boundaries. Part 2. Parallel motion. *J. Fluid Mech.* **99,** 755–783.

HAPPEL, J. & BRENNER, H. 1973 *Low Reynolds Number Hydrodynamics*. Noordhoff, Groningen, The Netherlands.

LADYZHENSKAYA, O. A. 1963 *The Mathematical Theory of Viscous Incompressible Flow*. Gordon & Breach, New York.

MIYAZAKI, T. & HASIMOTO, H. 1984 The motion of a small sphere in fluid near a circular hole in a plane wall. *J. Fluid Mech.* **145**, 201–221.

WANG, Y., KAO, J., WEINBAUM, S. & PFEFFER, R. 1986 On the inertial impaction of small particles at the entrance of a pore including hydrodynamic and molecular wall interaction effects. *Chem. Engng Sci.* **41**, 2845–2864.

YAN, Z. Y., WEINBAUM, S., GANATOS, P. & PFEFFER, R. 1987 The three dimensional hydrodynamic interaction of a finite sphere with a circular orifice at low Reynolds number. *J. Fluid Mech.* **174**, 39–68.

APPENDIX

We prove now the continuity requirements [16], [19] and [27] for the uniqueness of the solution. Let Ω_1 and Ω_2 be domains in R^3 such that $\Omega_1 \cap \Omega_2 = \varnothing$. Let Σ_1 be the boundary of Ω_1 and Σ_2 the boundary of Ω_2. Suppose that $\Sigma_1 \cap \Sigma_2 \neq \varnothing$ and that there exists a smooth surface Σ_3, $\Sigma_3 \subset \Sigma_1 \cap \Sigma_2$. We define a domain Ω, $\Omega = \Omega_1 \cup \Omega_2 \cup \Sigma_3$, with its boundary Σ, $\Sigma = \Sigma_1 \cup \Sigma_2 / \Sigma_3$; Ω may be unbounded.

Proposition

Let (U, p) be a solution of the Dirichlet problem of Stokes equation in Ω. Let (V^1, q^1) be a solution in Ω_1 such that $V^1|_{\Sigma_1/\Sigma_3} = U|_{\Sigma_1/\Sigma_3}$ and (V^2, q^2) a solution in Ω_2 such that $V^2|_{\Sigma_2/\Sigma_3} = U|_{\Sigma_2/\Sigma_3}$. In case Ω_1 or Ω_2 are unbounded we assume that these solutions vanish in infinity. Then, for (V^1, q^1) and (V^2, q^2) to coincide with (U, p) in Ω_1 and Ω_2 it is sufficient that

$$V_i^1|_{\Sigma_3} = V_i^2|_{\Sigma_3} \tag{A.1}$$

and that

$$\sigma_{ij}(V^1, q^1) n_j|_{\Sigma_3} = \sigma_{ij}(V^2, q^2) n_j|_{\Sigma_3}; \tag{A.2}$$

n_j is the unit normal vector to the smooth surface Σ_3 pointing either towards Ω_1 or towards Ω_2.

Proof

Let $D(f)$ be the energy dissipation function of the flow f, defined as

$$D(f) = \frac{\mu}{2} \int_\Omega \left(\frac{\partial f_i}{\partial x_j} + \frac{\partial f_j}{\partial x_i} \right) \left(\frac{\partial f_i}{\partial x_j} + \frac{\partial f_j}{\partial x_i} \right) \mathrm{d}x. \tag{A.3}$$

$D(f) = 0$ if either $f = 0$ or if f is a rigid-body motion. Define the flow (V, q) in Ω as

$$V_i(x) = \begin{cases} V_i^1 & x \in \Omega_1 \\ V_i^2 & x \in \Omega_2 \end{cases};$$

V_i is continuous across Σ_3. Since $(V_i - U_i) = 0$ on Σ, we get, by applying Gauss' theorem:

$$D(U - V) = \int_{\Sigma_3} \{(U_i - V_i)[\sigma_{ij}(U - V^1, p - q^1) - \sigma_{ij}(U - V^2, p - q^2)]\} n_j \, \mathrm{d}x \tag{A.4}$$

(n_j is the normal pointing towards Ω_2). Consequently, [A.1] and [A.2] imply that $D(U - V) = 0$. Hence the difference $U - V$ may be only a rigid-body motion but, since it vanishes on the boundary Σ, it must be zero.